

JGR Space Physics

RESEARCH ARTICLE

10.1029/2018JA026200

Key Points:

- Annual distribution of O_3^+ in Mars atmosphere
- Effect of dust on ozone distribution
- Modeling and SPICAM observations of ozone

Correspondence to:

S. A. Haider,
haider@prl.res.in

Citation:

Haider, S. A., Siddhi, Y. S., Masoom, J., & Bougher, S. (2019). Effect of dust storm and GCR impact on the production rate of O_3^+ in MY 28 and MY 29: Modeling and SPICAM observation. *Journal of Geophysical Research: Space Physics*, 124, 2271–2282. <https://doi.org/10.1029/2018JA026200>



Received 15 OCT 2018

Accepted 27 FEB 2019

Accepted article online 7 MAR 2019

Published online 25 MAR 2019

Effect of Dust Storm and GCR Impact on the Production Rate of O_3^+ in MY 28 and MY 29: Modeling and SPICAM Observation

S. A. Haider¹ , Y. S. Siddhi^{1,2}, J. Masoom^{1,2}, and S. Bougher³ 

¹Planetary Sciences Division, Physical Research Laboratory, Ahmedabad, India, ²Research Scholar, Faculty of Science, Pacific Academy of Higher Education of Research University, Udaipur, India, ³Climate and Space Sciences and Engineering, University of Michigan, Ann Arbor, Michigan, USA

Abstract We have developed a seasonally dependent energy loss model to calculate the zonally averaged production rates of O_3^+ due to impact of galactic cosmic rays in the dayside troposphere of Mars between solar longitudes (L_s) $\sim 0^\circ$ and 360° at low latitudes ($2^\circ N$, $2^\circ S$, $25^\circ N$, and $25^\circ S$), midlatitudes ($45^\circ N$ and $45^\circ S$), and high latitudes ($70^\circ N$ and $70^\circ S$) in the Martian Year (MY) 28 and MY 29. We also represent the seasonal variability of zonally averaged ozone column density obtained from Mars Climate Database (MCD; Millour et al., 2014, <https://hal.archives-ouvertes.fr/hal-01139592>) during the daytime. These results are compared with the daytime observations of column ozone made by Spectroscopy for the Investigation of the Characteristics of the Atmosphere of Mars onboard Mars Express (MEX). At mid-to-high latitudes ozone column density is maximum in northern winter and minimum in southern summer. At low-to-middle latitudes ($2^\circ N-S$, $25^\circ N-S$, and $45^\circ N-S$), the production rates of O_3^+ represent a broad peak between altitudes 26 and 45 km in both hemispheres. The peak production rates are increasing up to $L_s = 47.5^\circ$ and then stabilized at about $2.5 \times 10^{-8} \text{ cm}^{-3}/\text{s}$. At $L_s \geq 47.5^\circ$ the peak production rate of O_3^+ starts decreasing until it disappeared after $L_s = 127.5^\circ$. A major dust storm occurred in MY 28 at $L_s \sim 280^\circ$ in southern latitudes ($\sim 25^\circ - 35^\circ S$). During the dust storm period, dust opacity, ozone column density, and O_3^+ production rate on the surface of Mars were increased by a factor of ~ 3 .

1. Introduction

The O_3 molecule is formed from the product of O and O_2 by three-body reaction using CO_2 as third body. It is destroyed by hydrogen radicals. An anticorrelation between the abundances of ozone and water vapor exist in the atmosphere of Mars (Lefèvre et al., 2008). The neutral chemistry of O_3 has been discussed by several investigators in the Martian atmosphere (Lefèvre et al., 2004, 2008; Montmessin & Lefèvre, 2013). They have reported that O_3 column density is maximum at high latitude and minimum at low latitude. The ion chemistry of O_3^+ is not understood globally in the lower ionosphere of Mars. Ozone is very important for the negative ion chemistry of Mars. It plays a very important role in the formation of the *D* layer of the ionosphere and also affects the atmospheric electricity on Mars (Molina-Cuberos et al., 2002; Thomas & Gierasch, 1985). In the negative ion chemistry O^- is produced first by electron capture of O_3 . Later three-body reaction of CO_2 with O^- produces CO_3^- , which is associated with water and form a broad peak of water cluster ions $CO_3^-(H_2O)_n$ at about 30 km (Haider et al., 2007; Molina-Cuberos et al., 2002). This peak was first reported by Whitten et al. (1971) as a *D* layer in the lower ionosphere of Mars. The *D* layer occurs due to high efficiency of electron attachment to Ox molecules, which entails that the concentrations of negative ions are higher than that of electron below 30 km (Haider et al., 2009).

In presence of dust storms the production of O_3 is more which produces more negative ions $CO_3^-(H_2O)_n$ and increased the *D* layer of the Mars' ionosphere (cf. Michael et al., 2007; Molina-Cuberos et al., 2006; Tolendo-Redondo et al., 2017). During the dust storms dust aerosols are charged. The interaction of negative cluster ions $CO_3^-(H_2O)_n$ with positive charged aerosols reduced the *D* layer significantly (Haider et al., 2010). Therefore, *D* layer disappeared for few weeks until the dust storm settles down to the normal condition. Thus, the electron capture of O_3 is initially creating more negative cluster ions $CO_3^-(H_2O)_n$ in presence of dust storms when the concentrations of O_3 were increased significantly. Later the productions of $CO_3^-(H_2O)_n$ were destroyed due to their attachment with the positive charged aerosols.

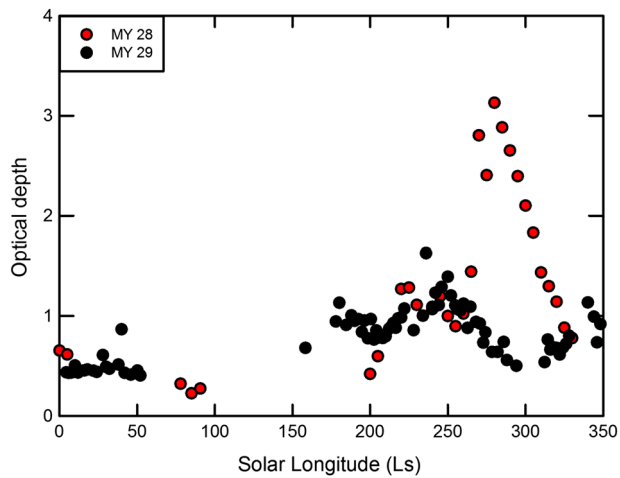


Figure 1. The annual seasonal variability of zonal mean UV dust optical depth observed by SPICAM in MY 28 and MY 29 at southern tropical region (25°–35°S).

Several dust storms have been observed on Mars in Martian year (MY) 10, MY13, MY25, and MY28 (Martin, 1984, 1995; Montabone et al., 2015; Smith et al., 2013). The Spectroscopy for the Investigation of the Characteristics of the Atmosphere of Mars (SPICAM) spectrometer onboard MEX has provided continuous observations of UV dust opacity (Montmessin et al., 2017). It has also observed column O_3 at different L_s , latitude, and longitude (Bertaux et al., 2006). The orbit of MEX does not change significantly with longitude (Smith et al., 2013). Therefore, we have averaged SPICAM observations over longitude for each L_s and latitude. These observations are compared with the zonally averaged ozone column densities obtained from MCD (Mars Climate database; website <http://www-mars.lmd.jussieu.fr>; Millour et al., 2014).

In the present paper we have also calculated annual seasonal dependence of the production rates of O_3^+ using energy loss model (Haider et al., 2007, 2008, 2009, 2015) due to impact of galactic cosmic rays (GCR) in the day-side troposphere of Mars in presence and absence of dust storm during MY28 and MY29, respectively. These production rates can be used in future for the global modeling of the D region ionosphere of Mars. It is

found that the production rates of O_3^+ are changing with season and produce a broad peak at low latitude between altitudes 30 and 40 km. The peak production rates of O_3^+ increases up to $L_s = 47.5^\circ$ while it decreases between $L_s = 47.5^\circ$ and $L_s = 127.5^\circ$. The O_3^+ production layer disappeared after $L_s = 127.5^\circ$. The production rates of O_3^+ were also enhanced significantly on the surface of Mars in MY28 during dust storm period when the optical depth of dust increased up to 3.

2. Motivation and Objectives

The nighttime measurements of ozone were carried out by SPICAM using the stellar occultation method (Montmessin & Lefèvre, 2013). This measurement cannot provide altitude profiles of ozone in the daytime atmosphere at altitude ≤ 60 –80 km where star signals are very weak (Bertaux et al., 2006). SPICAM also measured seasonal variability of ozone column abundance in the dayside atmosphere of Mars at different latitudes and longitudes. The column density of ozone varies strongly with latitudes and seasons. This is due to the fact that solar UV radiation is highest on average in the tropics and the large-scale air circulation in the troposphere slowly transports tropical ozone toward the pole. In presence of dust storm of MY28 ozone increases due to prominent drop of water abundance near the surface (Montmessin et al., 2017). This sudden decrease of water is also reported by Compact Reconnaissance Imaging Spectrometer (CRISM) during the dust storm of MY28 (Smith, 2009).

The seasonal cycle of Mars is dominated by a strong and asymmetric Hadley cell, extending between north and south midlatitudes producing trade winds and allowing cross-equatorial transport of dust and trace gases. The seasonal and latitudinal variability of ozone in MY 28 (in the presence of a dust storm) and MY 29 (in the absence of a dust storm) are not studied in detail during the daytime atmosphere of Mars. We have extended energy loss model of Haider et al. (2009) to calculate the production rates of O_3^+ in presence and absence of dust storms between $L_s = 0^\circ$ and 360° at low latitudes (2°N, 2°S, 25°N, and 25°S), midlatitudes (45°N and 45°S), and high latitudes (70°N and 70°S). The three main objectives of this paper are given below:

1. The column of ozone is observed in the daytime from the SPICAM instrument. We have compared seasonal variability of the ozone column observed by SPICAM with the model results of MCD in MY 28 and MY 29.
2. The annual variability of the production rate of O_3^+ is not measured or estimated in the daytime atmosphere of Mars. We have simulated altitude profiles of the production rate of O_3^+ during the daytime at different seasons and latitudes in MY 28 and MY 29.
3. The effect of a dust storm is a key problem in the lower atmosphere of Mars. We have studied seasonal and latitudinal dependence of the production rates of O_3^+ in presence and absence of a dust storm corresponding to MY 28 and MY 29, respectively.

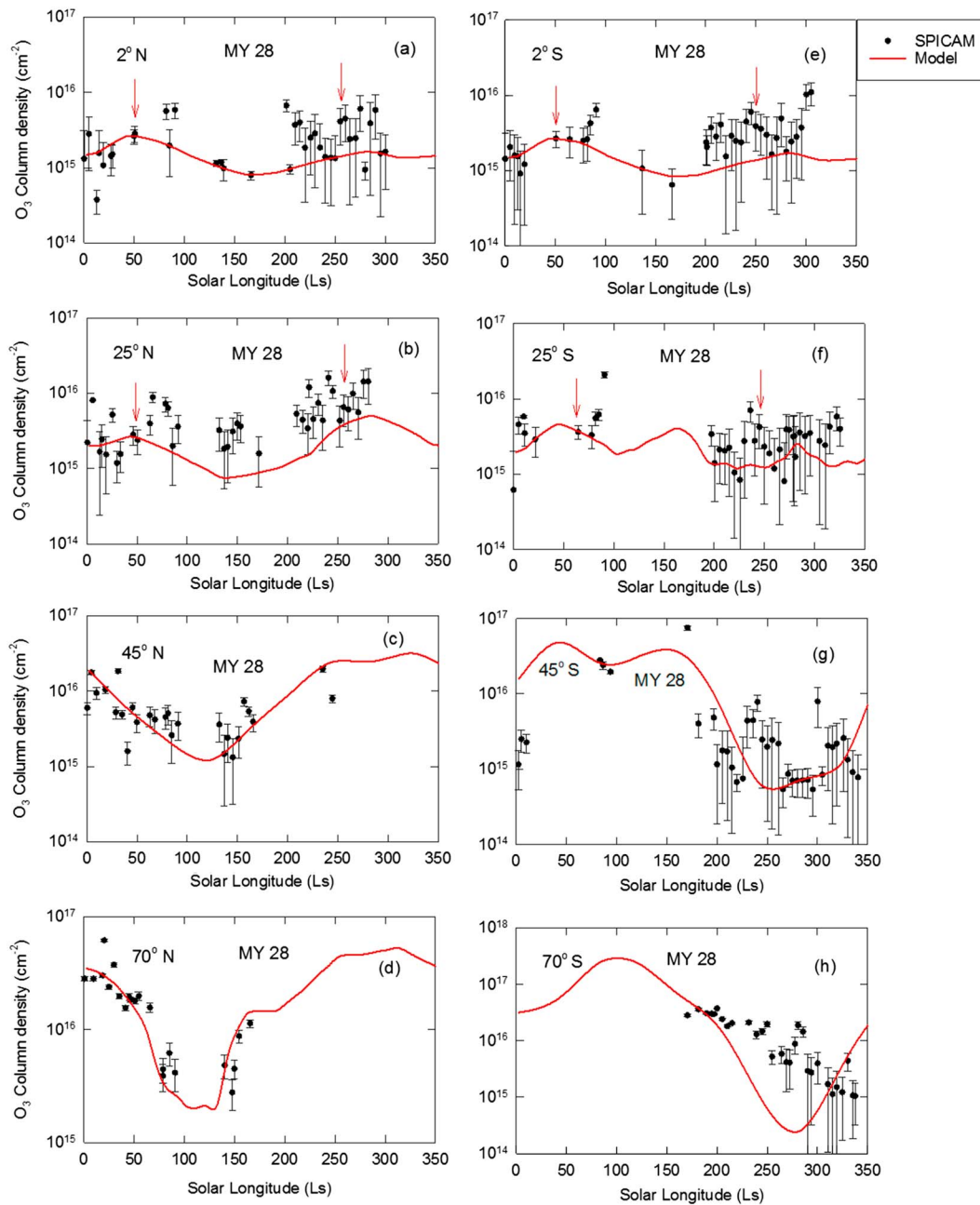


Figure 2. The annual seasonal variability of zonally averaged column ozone with error bars as observed by SPICAM in MY 28 at (a) 2°N, (b) 25°N, (c) 45°N, (d) 70°N, (e) 2°S, (f) 25°S, (g) 45°S, and (h) 70°S. These observations are compared with zonally averaged column ozone obtained from MCD model in MY 28. The arrow shows the two major peaks in ozone column cycle at $L_s \sim 50^\circ$ and $\sim 250^\circ$ in MY28 at latitudes 2°N, 2°S, 25°N, and 25°S in Figures 2a, 2e, 2b, and 2f, respectively.

3. Model

3.1. GCR Impact Ionization Rate

The impact of primary cosmic rays, mainly protons and particles onto the Martian atmospheric gases, produce protons, neutrons, and pions. Fast secondary nucleons can gain enough energy to increase the production of particles by neutral collisions. Neutral pions quickly decay to gamma rays, and their contribution to the energy deposition is very important in the lower atmosphere of Mars. At high altitude the maximum ion production rates are due to protons. Charged pions do not decay to muons before reaching the ground. Therefore, the muon energy is mainly transferred to the surface of Mars (Molina-Cuberos et al., 2002).

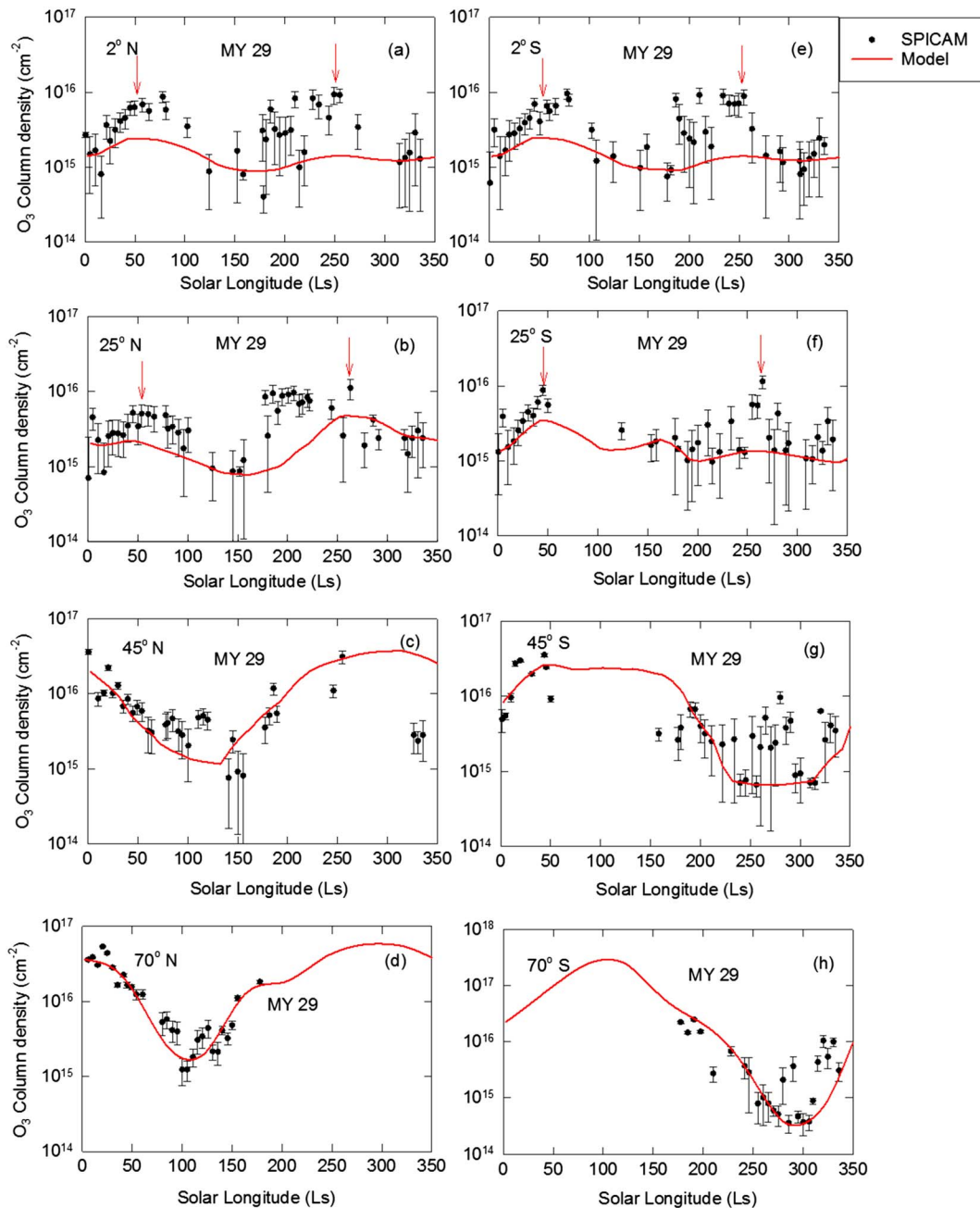


Figure 3. Same as in Figure 2 but for My 29.

Haider et al. (2007, 2009) used energy loss method and developed a GCR impact ionization model to calculate altitude profiles of ion production rates in the lower ionosphere of Mars. In this model the effects of seasonal and latitudinal variability were not included. This model is extended now and we have calculated altitude profiles of the ion production rate of O_3^+ at fixed latitudes for different seasons in MY28 and MY29. These calculations are made at low latitudes ($2^\circ N$, $2^\circ S$, $25^\circ N$, and $25^\circ S$), midlatitudes ($45^\circ N$ and $45^\circ S$), and high latitudes ($70^\circ N$ and $70^\circ S$) between $L_s \sim 0^\circ$ to 360° and altitude ~ 0 to 60 km. The 2° and 2 -km resolutions are taken for L_s and altitude distributions, respectively.

O'Brien et al. (1996) calculated the flux of unattenuated GCR from 10^3 to 10^{-5} particles·m⁻²·s⁻¹·GeV⁻¹·ster⁻¹ at energy interval of 1 to 1,000 GeV. We have assumed that this flux is precipitating into the lower atmosphere of Mars. We do not know what fraction of GCR impact at the top of the

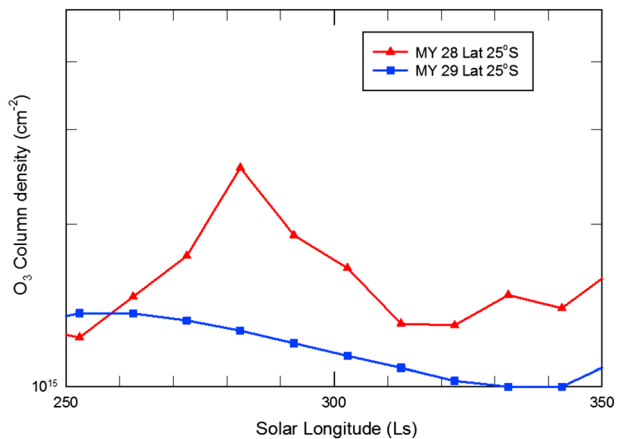


Figure 4. The zonal mean column ozone obtained from MCD model as a function of solar longitude (L_s) between $L_s = 250^\circ$ and $L_s = 350^\circ$ at latitude 25°S in MY 28 and My 29.

daytime atmosphere of Mars. In this model we have taken density profiles of O_3 from MCD for observing conditions of SPICAM. It should be noted that the unattenuated GCR flux does not depend on season and latitude; therefore, we have used the same flux in our calculation at different latitude and different solar longitudes. The modulation of cosmic rays is affected by the solar wind in the interplanetary medium. We have assumed that the solar wind interaction with cosmic rays is the same on Earth and Mars. Therefore, the same modulation of cosmic rays owing to the solar wind at Earth is used for Mars (Molina-Cuberos et al., 2002). GCR is ionizing all atmospheric gases. Since the goal of this paper is to study the global cycle of O_3^+ , therefore we have not included other gases of Mars in our model. Recently, the high-energy cosmic ray flux has been observed on the surface of Mars by the Radiation Assessment Detector (RAD) instrument onboard the Mars Science Laboratory (MSL; Ehresmann et al., 2014). We have not used this flux in our model because the RAD instrument observed mainly muon flux on the surface of Mars after attenuation of GCR through the atmosphere (Haider et al., 2015).

3.2. MCD Model

MCD is a database of Mars' meteorological fields derived from general circulation model (GCM). This model is validated using the available observed data (Millour et al., 2014). The GCM has been developed in the Laboratoire de Meteorologic Dynamique du CNRS (Paris, France) under the collaboration of Open University (UK), Oxford University (UK), Institute de Astrofisica de Andalucia (Spain), and Centre National d' Etudes Spatiales. MCD is freely available online for the use of atmospheric and environmental research of Mars (website <http://www-mars.lmd.jussieu.fr>). This model is developed for different scenarios of dust and solar conditions which are highly variable during short and long time scales. The UV radiation emitted from the Sun is varying due to solar flares, 27-day solar rotation, and the 11-year solar cycle. The atmosphere of Mars is also changing in the presence of low, medium, and high dust storm periods. In the MCD model, the climatology scenario, cold scenario, warm scenario, and dust scenario of the Mars atmosphere are provided for the modeling of the Martian ionosphere. In climatology scenario the solar minimum, medium, and maximum conditions are provided for the study of Mars' atmosphere. The low dust is considered in the cold scenario corresponding to an extremely clear atmosphere. For a given seasonal date (L_s) and location, the dust opacity is set to be the minimum observed over MY24–MY31. The warm scenario shows dusty atmosphere conditions but for a nonglobal dust storm period. The dust opacity at a given location and season is set to be the maximum observed over the MY 24–MY 31 except during the MY 25 and MY 28 intervals when global dust storms occurred. The effects of global dust storms are included in the dust scenario (the dust scenario represents the Mars' atmosphere in presence of global dust storms). The dust opacity is set to $\tau = 5$ during the dust storm period at a given location and season. Moreover, the dust optical properties are for this case set to represent "darker dust" than nominal (Wolff et al., 2009).

The MCD is based upon outputs from the LMD-MGCM model. The MGCM does include photochemistry; therefore, the empirical MCD model also includes the species from the MGCM outputs. The MCD included photochemistry, dynamics, and other metrological fields of the Martian atmosphere. These models calculate altitude profiles of air density; mixing ratios of CO_2 , O_2 , O , CO , O_3 , H , H_2 , N_2 , Ar , and H_2O ; neutral temperature; pressure and winds at different season; and latitude and longitude in the dayside and nightside atmosphere above the surface of Mars for different scenarios (as given above).

We have taken altitude profiles (0 to 60 km) of ozone from the MCD model at low latitudes (2°N , 2°S , 25°N , and 25°S), midlatitudes (45°N and 45°S), and high latitudes (70°N and 70°S) between $L_s \sim 0^\circ$ and 360° for dust storm and cold scenarios that occurred in MY 28 and MY 29, respectively. During MY 28 the density of ozone is larger by a factor of ~ 3 than that estimated for MY 29 (Millour et al., 2014). These densities are averaged over longitude. Later the zonally averaged profiles of ozone were integrated over altitude and compared with global cycle of column ozone density observed by SPICAM. This experiment also measured the vertical profiles of ozone in the nighttime atmosphere of Mars between altitude ~ 20 and ~ 70 km from the stellar occultation method (Lebonnois et al., 2006; Montmessin & Lefèvre, 2013). No ozone was detected

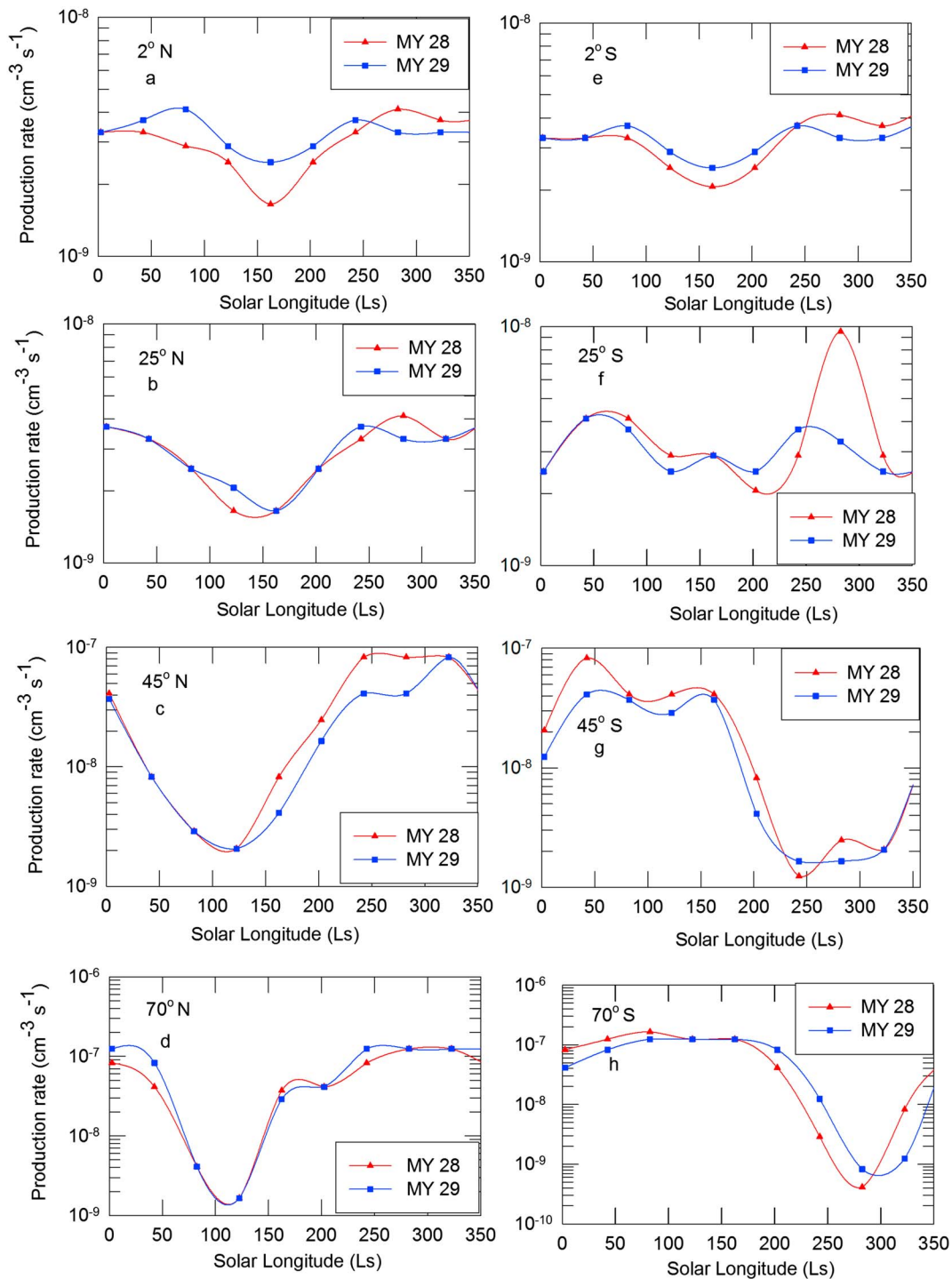


Figure 5. The annual variability of zonal mean production rates of O_3^+ on the surface of Mars in MY 28 and MY 29 at latitudes (a) $2^\circ N$, (b) $25^\circ N$, (c) $45^\circ N$, (d) $70^\circ N$, (e) $2^\circ S$, (f) $25^\circ S$, (g) $45^\circ S$, and (h) $70^\circ S$.

from this method down to ~ 20 – 30 -km altitude. Ozone was also detected in the Martian atmosphere by Mariner 7 and 9 using Ultraviolet Spectrometers (Barth et al., 1973; Barth & Hord, 1971). The altitude profiles of ozone are not measured in the daytime atmosphere of Mars. MCD has provided a complete set of global data of O_3 abundance during the daytime and nighttime atmosphere of Mars at all altitudes, latitudes, and longitudes for different atmospheric conditions. Our objective is to study seasonal and

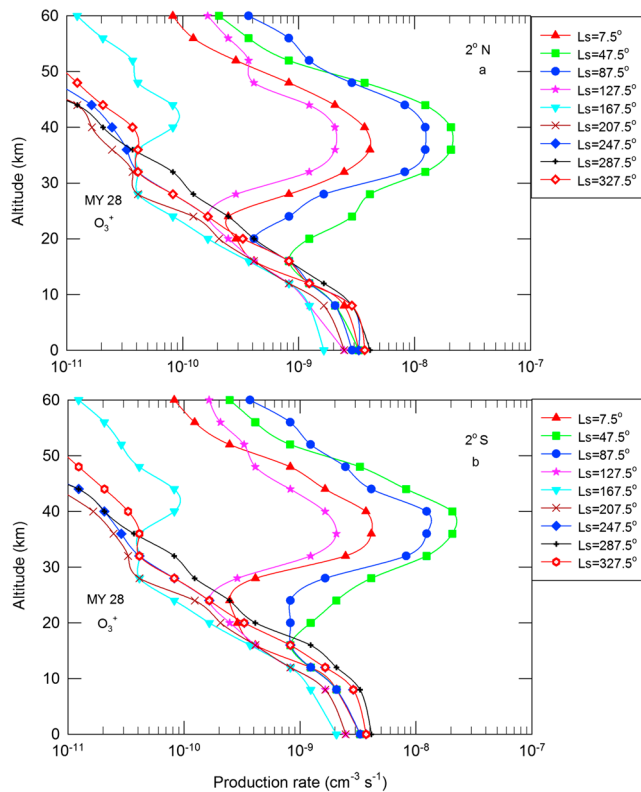


Figure 6. The altitude profiles of the production rates of O_3^+ in MY 28 at latitudes (a) $2^\circ N$ and (b) $2^\circ S$ for $L_s = 7.5^\circ, 47.5^\circ, 87.5^\circ, 127.5^\circ, 167.5^\circ, 207.5^\circ, 247.5^\circ, 287.5^\circ,$ and 327.5° .

altitude variability of the production rates of O_3^+ during the daytime above the surface of Mars in the presence and absence of dust storm in MY28 and MY29, respectively. In this model calculation daytime altitude profiles of ozone between 0 and 60 km at low latitudes ($2^\circ N, 2^\circ S, 25^\circ N,$ and $25^\circ S$), midlatitudes ($45^\circ N$ and $45^\circ S$), and high latitudes ($70^\circ N$ and $70^\circ S$) for $L_s \sim 0$ to 360° are required. Therefore, we have not used nighttime density profiles of ozone observed by SPICAM in our model. The MCD model is providing all required inputs and can serve the objectives of this paper.

4. Results and Discussion

There have been observed several dust storms on Mars. Mariner 9 and Viking have detected two major dust storms in MY 10 and MY 13, respectively (Martin, 1984, 1995). The infrared optical depths were increased to ~ 1.5 to 2.6 during these dust storms period. After two decades, the continuous remote sensing observations of infrared dust optical depths were carried out during MY 24 to MY 32 from MGS and Mars Odyssey spacecraft (Montabone et al., 2015). During these periods two major dust storms were observed in MY 25 and MY 28 with opacities 1.7 and 1.2 at $L_s \sim 210^\circ$ and 280° , respectively (Montabone et al., 2015; Sheel & Haider, 2016). Recently, a new global dust storm has been detected by the Opportunity Mars Exploration Rover (MER) and the Mars Reconnaissance Orbiter (MRO) in June 2018 (MY34; <https://mars.nasa.gov/resources/21917/atmospheric-opacity-from-opportunitys-point-of-view>). The previous dust storms in MY 10, MY 13, MY 25, and MY 28 were slower to build in comparison to the new dust storm of MY 34. The new dust storm observed maximum UV dust opacity $\tau = 10.8$ on 10 June 2018 at about $L_s \sim 190^\circ$ and spread quickly all over the globe

(<https://www.nasa.gov/news/news.php>). Our model result is dedicated to the previous dust storm ($\tau = 1.2$) that occurred in MY 28 at the southern tropical region ($25^\circ\text{--}35^\circ S$).

Figure 1 represents seasonal variability of zonal mean UV dust opacity measured by SPICAM in MY 28 and MY 29 (Holmes et al., 2018) at the southern tropical region ($25^\circ\text{--}35^\circ S$). These observations have been carried out from the nadir direction. The optical depths are averaged over longitude. It is found that the dust optical depth increased by a factor of ~ 3 on the surface of Mars during southern summer at $L_s \sim 280^\circ$ in MY 28. The minimum visible opacity of dust is observed $\sim 0.2 \mu m$ in the cleaner southern winter season. The regional dust storms occurred in different seasons of Mars at optical depth $\tau = 0.5$ to 0.75 between $L_s \sim 0^\circ\text{--}50^\circ, 200^\circ,$ and $L_s \sim 275^\circ\text{--}350^\circ$. In this dust storm a large amount of dust lifted up into the atmosphere and formed two distinct layers at altitude range $\sim 20\text{--}30$ and $\sim 45\text{--}65$ km (Haider et al., 2015). These dust layers have been observed by CRISM and Mars Climate Sounder (MCS) onboard Mars Reconnaissance Orbiter (Guzewich et al., 2014; Heavens et al., 2014) (it should be noted that the dust optical depths obtained from SPICAM are generally larger than the results obtained from MER, MCS, and CRISM (Willame et al., 2017)).

The total amount of O_3 in the atmosphere of Mars undergoes seasonal variation due to formation of the polar caps. Figures 2a–2h and 3a–3h represent the seasonal variability of zonally averaged column ozone observed by SPICAM in MY 28 and MY 29, respectively, at low latitudes ($2^\circ N, 2^\circ S, 25^\circ N,$ and $25^\circ S$), midlatitudes ($45^\circ N$ and $45^\circ S$), and high latitudes ($70^\circ N$ and $70^\circ S$). These observations are compared with the zonally averaged column ozone obtained from MCD in MY 28 and MY 29. The comparison of year-to-year seasonal variability in column ozone shows strong similarity in MY 28 and MY 29 except at $L_s \sim 280^\circ$ during the dust storm period which occurred in MY 28 at southern latitudes $\sim 25^\circ\text{--}35^\circ S$. The seasonal change in column ozone is low at low latitudes, but at high latitudes it is chaotic and indicates that atmospheric ozone is highly perturbed.

At low latitudes ($2^\circ N, 2^\circ S, 25^\circ N,$ and $25^\circ S$) the observations do not match so well with the MCD model underestimating column ozone by $\sim 20\%$. The disagreement between observation and model at low

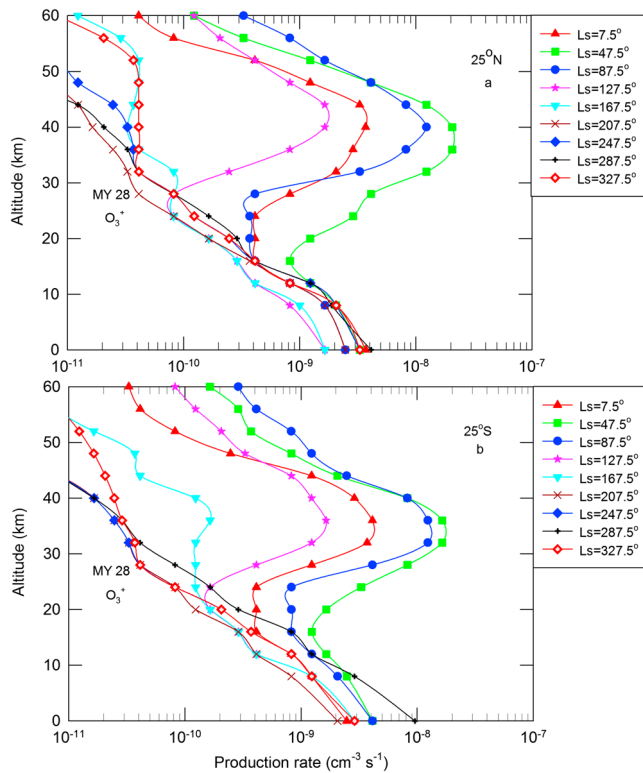


Figure 7. Same as in Figure 6 but for latitudes (a) 25°N and (b) 25°S.

latitudes may be associated due to several reasons as given below: (1) the excessive transport of water vapor from Tharsis and Arabia Terrain can reduce column ozone in the model (Steele et al., 2014), (2) modeling biases in water vapor can also explain the underestimation of total ozone at low-latitude region (Holmes et al., 2018), and (3) the SPICAM measurements have large error on the order of $1\text{--}5 \times 10^{15}$ molecules/cm² (Lebonnois et al., 2006). The estimated column densities of ozone are varying within this error bar at low-latitude region and (4) ozone can also be affected by topography of Mars through the effect of gravity waves. An increase in O₃ column over Hellas basin in SPICAM measurements is attributed to a topographical induced transport of the polar air (Clancy et al., 2016). In Figures 2a–2e and 2b–2f we have plotted SPICAM and MCD profiles of ozone column density for their comparison in MY28 between northern and southern hemispheres at low latitudes 2°N–S and 25°N–S, respectively. Similarly in Figures 3a–3e and 3b–3f we have also plotted SPICAM and MCD profiles of ozone column density for their comparison in MY29 between northern and southern hemispheres at low latitudes 2°N–S and 25°N–S, respectively. In these figures two broad peaks (marked by arrow) are measured in the column ozone cycle with values $\sim 5 \times 10^{15}$ and $\sim 1 \times 10^{16}$ cm⁻² at $L_s \sim 50^\circ$ and $L_s \sim 250^\circ$, respectively. These peak values are larger by a factor of 5–10 than that produced by MCD model. In Figure 2f MCD model represents a third peak in the column ozone density with a value $\sim 2 \times 10^{15}$ cm⁻² between L_s 150° and 175°. This peak may be produced due to the effect of regional dust storm on the ozone column density. The global dust storm of MY28 has been suggested to have several regional dust storms before the major dust storm (Sheel & Haider, 2016).

These major and regional dust storms have produced ~ 50 and $\sim 30\%$ reductions in the measured total water vapor content at $L_s \sim 280^\circ$ and 175° , respectively (Trokhimovskiy et al., 2015). There is an anticorrelation between the abundances of ozone and water vapor. Therefore, the calculated column density of O₃ may increase in Figure 2f due to the effect of regional dust storm between $L_s = 150^\circ$ and 175° . It should be noted that the SPICAM data are not available between L_s 100° and 200° at latitude 25°; therefore, third peak is not observed in Figure 2f.

At mid-to-high latitudes (45°N, 45°S, 70°N, and 70°S) the ozone column densities are maximum in northern winter and minimum in southern summer. In both hemispheres the column densities of ozone are lower at midlatitudes by a factor of 2–5 than the column densities of ozone at high latitudes. In northern hemisphere the ozone is not measured between $L_s \sim 250^\circ$ and 350° at mid-to-high latitudes. At these latitudes the seasonal profiles of column ozone obtained from MCD are generally in good agreement with the SPICAM observations except in Figures 2h and 3h at latitude 70°S. In these figures we notice that the column ozone observed by SPICAM in MY28 and MY29 are higher than the MCD-derived column ozone by a factor of ~ 5 to 8 between L_s 230°–300° and 300°–330°, respectively. This enhancement in the column ozone was observed due to high dust opacity ~ 1.5 (Willame et al., 2017).

Figure 4 represents zonal mean column ozone obtained from MCD as a function of solar longitude between $L_s \sim 250^\circ$ and 350° at latitude 25°S in MY 28 and MY 29. In presence of the dust storm a major dust layer is formed above the surface of Mars (Guzewich et al., 2014; Haider et al., 2015; Heavens et al., 2014). During the thick layer of dust, the sunlight cannot penetrate deep into the atmosphere of Mars. This interrupts the dissociation of ozone below the dust layer, which is the main loss mechanism of ozone in dayside atmosphere. On the other hand, production of O₃ is directly related to the production of the oxygen atom, which is produced more above the dust layer from the photolysis of CO₂. Therefore, the integrated column O₃ will be enhanced during the dust storm period. In Figure 4 we have found that O₃ column density is enhanced by a factor of ~ 2.6 at $L_s \sim 280^\circ$ during the dust storm of MY28. Recently, Liu et al. (2018) have observed neutral densities of CO₂, Ar, N₂, CO, and O at high altitudes from 170 to 220 km in response to dust increases in the lower atmosphere, observed by the in situ Neutral Gas Ion Mass Spectrometer onboard the Mars

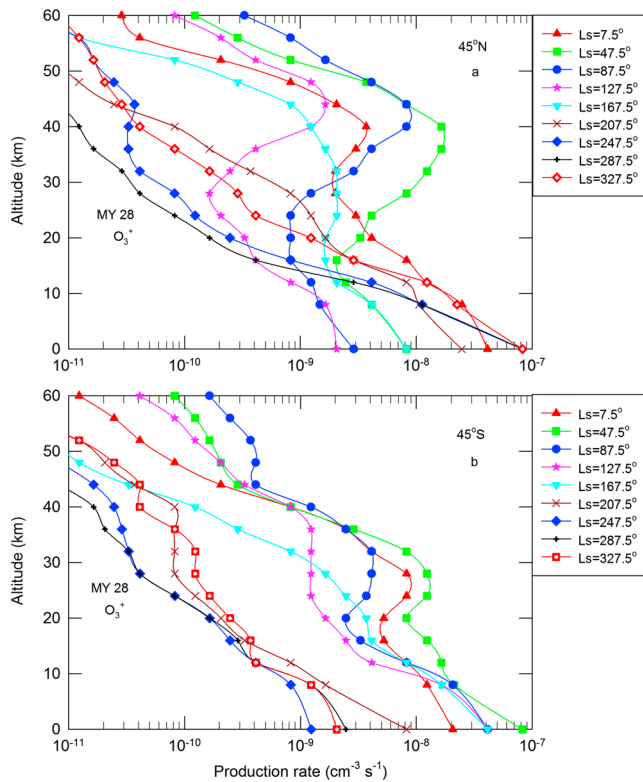


Figure 8. Same as in Figure 6 but for latitudes (a) 45°N and (b) 45°S.

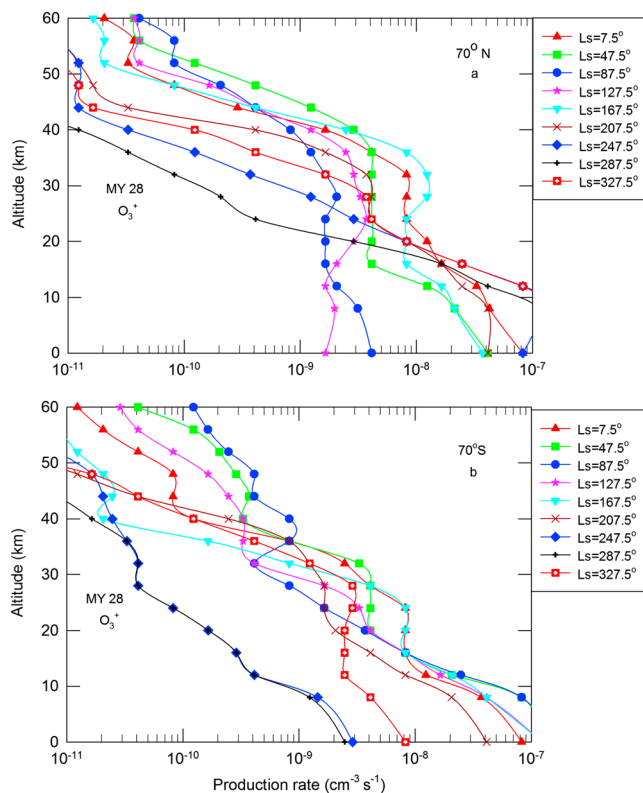


Figure 9. Same as in Figure 6 but for latitudes (a) 70°N and (b) 70°S.

Atmosphere and Volatile Evolution (MAVEN) satellite. These observations reveal that the densities of all atmospheric gases increase up to ~200% in the presence of dust storm. The thermospheric density increases caused by dust have also been reported earlier using the observations made by Accelerometer experiment onboard MGS (Bougher et al., 1999, 2017; Keating et al., 1998).

Figures 5a–5h represent the annual variability of the zonal mean production rates of O_3^+ on the surface of Mars in MY 28 and MY 29 at four low latitudes (2°N, 2°S, 25°N and 25°S), two midlatitudes (45°N and 45°S) and two high latitudes (70°N and 70°S). These production rates are estimated from the seasonally dependent energy loss model by using MCD model-derived ozone column densities. At mid-to-high latitudes (Figures 5c, 5d, 5g, and 5h) maximum and minimum ion production rates are calculated during northern winter and southern summer, respectively, while minimum and maximum ion production rates were estimated during northern summer and southern winter, respectively. At low northern and southern latitudes (Figures 5a, 5b, 5e, and 5f) two crests and one trough are produced in each annual cycle of the production rates of O_3^+ at $L_s \sim 50^\circ\text{--}100^\circ$, $L_s \sim 200^\circ\text{--}300^\circ$, and $L_s \sim 150^\circ$, respectively. These crests and trough are produced at low latitudes due to the Hadley asymmetric circulation (cf. Millour et al., 2014). The annual cycle of the production rates of O_3^+ are nearly same in MY28 and MY29 except for the dust storm period as shown in Figure 5f. This is due to the fact that MCD-derived column density of O_3 is enhanced between $L_s = 250^\circ$ and $L_s = 350^\circ$ at latitude 25°S in MY28 (see Figure 4). In Figure 5f, we have used this column density of O_3 for the calculation of the ion production rate of O_3^+ .

Since the altitude profiles of the production rates of O_3^+ are nearly same in MY 28 and MY 29 at the same latitudes and same seasons we have plotted these profiles in Figures 6a, 6b, 7a, 7b, 8a, 8b, 9a, and 9b at latitudes 2°N–S, 25°N–S, 45°N–S, and 70°N–S, respectively, for MY 28 only. In Figures 6a, 7a, 8a, and 9a we represent the altitude profiles of the production rates of O_3^+ at northern latitudes 2°N, 25°N, 45°N, and 70°N, respectively, for $L_s \sim 7.5^\circ, 47.5^\circ, 87.5^\circ, 127.5^\circ, 167.5^\circ, 207.5^\circ, 247.5^\circ, 287.5^\circ,$ and 327.5° . Figures 6b, 7b, 8b, and 9b represent the same profiles of the production rates of O_3^+ but at southern latitudes 2°S, 25°S, 45°S, and 70°S, respectively. Table 1 represents the peak altitudes and peak production rates of O_3^+ in MY28 at $L_s \sim 7.5^\circ, 47.5^\circ, 87.5^\circ,$ and 127.5° for latitudes 2°N–S, 25°N–S, and 45°N–S. At these latitudes the peak production rates of O_3^+ increased up to $L_s \sim 47.5^\circ$ with maximum value $\sim 2.5 \times 10^{-8} \text{ cm}^{-3}/\text{s}$. Later it decreased up to $L_s \sim 127.5^\circ$ and then disappeared at $L_s \sim 167.5^\circ, 207.5^\circ, 247.5^\circ, 287.5^\circ,$ and 327.5° . The clear peaks are found in these production rates between altitudes 26 and 45 km. The production layer of O_3^+ is higher in altitude at low latitudes and lower in altitude at midlatitudes, especially in southern region. The ionization peaks do not occur in the troposphere of Mars at polar latitudes $\sim 70^\circ\text{N}$ and 70°S .

At latitudes 45°N, 45°S, 70°N, and 70°S the surface production rates of O_3^+ are increasing by 2 orders of magnitude in northern winter due to condensation of CO_2 frost. At these latitudes the surface production rates of O_3^+ are decreasing by 2 orders of magnitude in southern summer due to sublimation of CO_2 frost. During summer, polar caps are releasing water vapor which destroys the ozone (Lefèvre et al., 2008). This process does

Table 1
Peak Altitudes and Peak Production Rate of O_3^+ in MY 28

Latitude	L_s	Peak Altitude (km)	Peak Production Rate (cm^{-3}/s)
2°N	7.5°	35	4.0×10^{-9}
	47.5°	40	2.5×10^{-8}
	87.5°	38	1.3×10^{-8}
	127.5°	36	2.0×10^{-9}
2°S	7.5°	36	4.1×10^{-9}
	47.5°	39	2.5×10^{-8}
	87.5°	36	1.2×10^{-8}
	127.5°	37	2.0×10^{-9}
25°N	7.5°	42	4.0×10^{-9}
	47.5°	39	2.0×10^{-8}
	87.5°	41	1.5×10^{-8}
	127.5°	45	2.0×10^{-9}
25°S	7.5°	38	4.1×10^{-9}
	47.5°	36	1.6×10^{-8}
	87.5°	39	1.2×10^{-8}
	127.5°	40	1.6×10^{-9}
45°N	7.5°	40	3.5×10^{-9}
	47.5°	42	1.5×10^{-8}
	87.5°	43	1.0×10^{-8}
	127.5°	41	1.8×10^{-9}
45°S	7.5°	26	1.0×10^{-8}
	47.5°	30	1.5×10^{-8}
	87.5°	28	4.0×10^{-9}
	127.5°	32	1.2×10^{-9}

not occur in northern polar winter which is too cool and protected from the formation of odd hydrogen species, which significantly contributes in the destruction of ozone. The ozone concentration peak at low-to-middle latitudes can be obtained in both hemispheres between altitudes 25 and 45 km at $L_s \sim 7.5^\circ, 47.5^\circ, 87.5^\circ,$ and 127.5° from the photolysis of O_2 which combines with O and forms the O_3 layer (Lefevre et al., 2004). This layer is fully destroyed by photodissociation. These peak heights are reduced by about 10–20 km at southern midlatitudes in comparison to northern midlatitudes. These peaks are not found in the production rates of O_3^+ at high latitudes in all seasons of both hemispheres.

The SPICAM has observed two distinct ozone layers in the nighttime atmosphere of Mars at low-to-middle latitudes (Lebonnois et al., 2006). The first layer occurred near the surface. The second layer was observed between altitudes 25 and 60 km. Later Montmessin and Lefèvre (2013) observed a broad peak in the vertical profiles of ozone at altitudes between 40 and 60 km in southern polar night, which was overlooked by Lebonnois et al. (2006). The nighttime ozone layer is produced due to horizontal transport of oxygen atoms from the dayside into the nightside atmosphere across the terminator (Montmessin & Lefèvre, 2013). We have not detected any peak in the daytime vertical profiles of the production rates of O_3^+ near the surface. Our study suggests that the mechanisms of ozone formation in the dayside and nightside atmosphere of Mars are different at low, middle, and high latitudes. The dust increases the ion production rate by a factor of 3–4 on the surface in MY 28 (Figure 5f). The effects of dust on the production rate is nearly absent beyond ~10-

km altitude (Figure 7b). The peak production rate of O_3^+ is directly correlated with the abundance of ozone. GCR does not produce ionization peaks but it is attenuated throughout the atmosphere in the production rates of O_3^+ .

5. Summary and Conclusions

We have developed a seasonally dependent energy loss model to study the annual variability of the ion production rates of O_3^+ due to impact of GCR in the daytime ionosphere of Mars at low, middle, and high latitudes. These calculations are carried out in MY 28 and MY 29 between $L_s \sim 0^\circ$ to 360° and altitudes 0 to 60 km at latitudes 2°N–S, 25°N–S, 45°N–S, and 70°N–S. We also represent seasonal variability of zonal mean ozone column density obtained from the MCD model at different latitudes in MY 28 and MY 29. These results are compared with the daytime observations of the column ozone made by SPICAM onboard MEX. It is found that the ozone column density maximizes in northern winter and minimizes in southern summer at mid-to-high latitudes. The ion production rates of O_3^+ represent a broad peak between 30 and 40 km in both hemispheres at low-to-middle latitudes. The peak production rates are increasing up to $L_s = 47.5^\circ$ and then decreasing until they disappear after $L_s = 127.5^\circ$. There are no ionization peaks in these production rates at polar latitudes.

A major dust storm occurred in MY 28 at $L_s \sim 280^\circ$ in southern tropical latitudes (25°–35°S). During the storm period the dust opacity, ozone column density and production rates of O_3^+ were increased on the surface of Mars by a factor of 3–4. The altitude profiles of ozone are not measured in the daytime atmosphere of Mars. These profiles are measured in the nighttime only by the stellar occultation method (Montmessin & Lefèvre, 2013). Using a detailed computational study of seasonal dependent energy loss model we found that the production rates of O_3^+ are strongly changing with season and latitude due to different chemical processes of ozone formation in the daytime atmosphere of Mars. The mechanisms of ozone layer formation are substantively different in different seasons at low, middle, and high latitudes. This theoretical prediction awaits experimental validation and in the absence of ozone measurements in the dayside atmosphere of Mars, our results can serve as a benchmark that can guide the design of future payloads of ozone measurements on Mars.

Acknowledgments

SPICAM instrument was designed and fabricated by three institutes: Service d'Aéronomie, France; BIRA, Belgium; and IKI, Moscow. We wish to express our gratitude to all members of SPICAM team who participated in this project. SPICAM data have been provided to us by F. Lefevre (franck.lefevre@aero.jussieu.fr) and are freely available at ftp://psa.esac.int/pub/mirror/MARS-EXPRESS/SPICAM/. We also thank to F. Lefevre and his team for their support. Authors also acknowledge MCD data team: E. Millour (millour@lmd.jussieu.fr) and F. Forget (francois.forget@lmd.jussieu.fr) for providing freely accessible Mars Climate data at http://www-mars.lmd.jussieu.fr. S.A. Haider and Y. Siddhi acknowledge the support of J.C. Bose grant for supporting to carry out this work.

References

Barth, C. A., & Hord, C. W. (1971). Mariner ultraviolet spectrometer: Topography and polar cap. *Science*, *173*(3993), 197–201. <https://doi.org/10.1126/science.173.3993.197>

Barth, C. A., Hord, C. W., Stewart, A. I., Lane, A. L., Dick, M. L., & Anderson, G. P. (1973). Mariner 9 ultraviolet spectrometer experiment: Seasonal variation of ozone on Mars. *Science*, *179*(4075), 795–796. <https://doi.org/10.1126/science.179.4075.795>

Bertaux, J. L., Korabiev, O., Perrier, S., Quemerais, E., Montmessin, F., Leblanc, F., et al. (2006). SPICAM onboard Mars Express: Observing modes, and overview of typical results. *Journal of Geophysical Research*, *111*, E10S90. <https://doi.org/10.1029/2006JE002690>

Bougher, S. W., Engel, S., Roble, R. G., & Foster, B. (1999). Comparative terrestrial planet thermospheres: 2. Solar cycle variation of global structure and winds at equinox. *Journal of Geophysical Research*, *104*(E7), 16,591–16,611. <https://doi.org/10.1029/1998JE001019>

Bougher, S. W., Roeten, K. J., Olsen, K., Mahaffy, P. R., Benna, M., Elrod, M., et al. (2017). The structure and variability of Mars dayside thermosphere from MAVEN NGIMS and IUVS measurements: Seasonal and solar activity trends in scale heights and temperatures. *Journal of Geophysical Research: Planets*, *122*, 1296–1313. <https://doi.org/10.1002/2016JA023454>

Clancy, R. T., Wolff, M. J., Lefèvre, F., Cantor, B. A., Malin, M. C., & Smith, M. D. (2016). Daily global mapping of Mars ozone column abundances with MARCI UV band imaging. *Icarus*, *266*, 112–133. <https://doi.org/10.1016/j.icarus.2015.11.016>

Ehresmann, B., Zeitlin, C., Hassler, D. M., Wimmer-Schweingruber, R. F., Böhm, E., Böttcher, S., et al. (2014). Charged particle spectra obtained with the Mars Science Laboratory Radiation Assessment Detector (MSL/RAD) on the surface of Mars. *Journal of Geophysical Research: Planets*, *119*, 468–479. <https://doi.org/10.1002/2013JE004547>

Guzewich, S. D., Smith, M. D., & Wolff, M. J. (2014). The vertical distribution of Martian aerosol particle size. *Journal of Geophysical Research: Planets*, *119*, 2694–2708. <https://doi.org/10.1002/2014JE004704>

Haider, S. A., Abdu, M. A., Batista, I. S., Sobral, J. H., Luan, X., Kallio, E., et al. (2009). D, E, and F layers in the daytime at high-latitude terminator ionosphere of Mars: Comparison with Earth's ionosphere using COSMIC data. *Journal of Geophysical Research*, *114*, A03311. <https://doi.org/10.1029/2008JA013709>

Haider, S. A., Batista, I. S., Abdu, M. A., Muralikrishna, P., Shah, S. Y., & Kuroda, T. (2015). Dust storm and electron density in the equatorial D region ionosphere of Mars: Comparison with Earth's ionosphere from rocket measurements in Brazil. *Journal of Geophysical Research: Planets*, *120*, 8968–8977. <https://doi.org/10.1002/2015JA021630>

Haider, S. A., Sheel, V., Singh, V., Maguire, W. C., & Molina-Cuberos, G. J. (2008). Model calculation of production rates, ion and electron densities in the evening troposphere of Mars at latitudes 67°N and 62°S: Seasonal variability. *Journal of Geophysical Research*, *113*, A08320. <https://doi.org/10.1029/2007JA012980>

Haider, S. A., Sheel, V., Smith, M. D., Maguire, W. C., & Molina-Cuberos, G. J. (2010). Effect of dust storm on the D region of the Martian ionosphere: Atmospheric electricity. *Journal of Geophysical Research*, *115*, A12336. <https://doi.org/10.1029/2010JA016125>

Haider, S. A., Singh, V., Choksi, V. R., Maguire, W. C., & Verigin, M. I. (2007). Calculated densities of H₃O⁺(H₂O)_n, NO₂⁻(H₂O)_n, CO₃⁻(H₂O)_n and electron in the nighttime ionosphere of Mars: Impact of solar wind electron and galactic cosmic rays. *Journal of Geophysical Research*, *112*, A12309. <https://doi.org/10.1029/2007JA012530>

Heavens, N. G., Johnson, M. S., Abdou, W. A., Kass, D. M., Kleinböhl, A., McCleese, D. J., et al. (2014). Seasonal and diurnal variability of detached dust layers in the tropical Martian atmosphere. *Journal of Geophysical Research: Planets*, *119*, 1748–1774. <https://doi.org/10.1002/2014JE004619>

Holmes, J. A., Lewis, S. R., Patel, M. R., & Lefèvre, F. (2018). First ozone reanalysis on Mars using SPICAM data. In: From Mars Express to ExoMars, 27–28 Feb 2018, Madrid.

Keating, G. M., Bougher, S. W., Zurek, R. W., Tolson, R. H., Cancro, G. J., Noll, S. N., et al. (1998). The structure of the upper atmosphere of Mars: In situ accelerometer measurements from Mars Global Surveyor. *Science*, *279*(5357), 1672–1676. <https://doi.org/10.1126/science.279.5357.1672>

Lebonnois, S., Quemerais, E., Montmessin, F., Lefèvre, F., Perrier, S., Bertaux, J. L., & Forget, F. (2006). Vertical distribution of ozone on Mars as measured by SPICAM/Mars Express using stellar occultations. *Journal of Geophysical Research*, *111*, E09S05. <https://doi.org/10.1029/2005JE002643>

Lefèvre, F., Bertaux, J. L., Clancy, R. T., Encrenaz, T., Fast, K., Forget, F., et al. (2008). Heterogeneous chemistry in the atmosphere of Mars. *Nature*, *454*(7207), 971–975. <https://doi.org/10.1038/nature07116>

Lefèvre, F., Lebonnois, S., Montmessin, F., & Forget, F. (2004). Three-dimensional modeling of ozone on Mars. *Journal of Geophysical Research*, *109*, E07004. <https://doi.org/10.1029/2004JE002268>

Liu, G., England, S. L., Lillis, R. J., Withers, P., Mahaffy, P. R., Rowland, D. E., et al. (2018). Thermospheric expansion associated with dust increase in the lower atmosphere on Mars observed by MAVEN/NGIMS. *Geophysical Research Letters*, *45*, 2901–2910. <https://doi.org/10.1002/2018GL077525>

Martin, L. J. (1984). Clearing the Martian air: The troubled history of dust storms. *Icarus*, *57*(3), 317–321. [https://doi.org/10.1016/0019-1035\(84\)90120-9](https://doi.org/10.1016/0019-1035(84)90120-9)

Martin, T. Z. (1995). Mass of dust in the Martian atmosphere. *Journal of Geophysical Research*, *100*(E4), 7509–7512. <https://doi.org/10.1029/95JE00414>

Michael, M., Barani, M., & Tripathi, S. N. (2007). Numerical predictions of aerosol charging and electrical conductivity of the lower atmosphere of Mars. *Geophysical Research Letters*, *34*, L04201. <https://doi.org/10.1029/2006GL028434>

Millour, E., Forget, F., Spiga, A., Navarro, T., Madeleine, J.-B., Pottier, A., et al. (2014). A new Mars climate database v5.1, paper 1301 presented at The Fifth International Workshop on Mars Atmosphere: Modeling and Observations, Oxford, U. K., Jan. 2014.

Molina-Cuberos, G. J., Lichtenegger, H., Schwingenschuh, K., López Moreno, J. J., & Rodrigo, R. (2002). Ion neutral chemistry model of the lower ionosphere of Mars. *Journal of Geophysical Research*, *107*(E5), 5027. <https://doi.org/10.1029/2000JE001447>

Molina-Cuberos, G. J., Morente, J. A., Besser, B. P., Porti, J., Lichtenegger, H., Schwingenschuh, K., et al. (2006). Schumann resonances as a tool to study the lower ionospheric structure of Mars. *Radio Science*, *41*, RS1003. <https://doi.org/10.1029/2004RS003187>

Montabone, L., Forget, F., Millour, E., Wilson, R. J., Lewis, S. R., Cantor, B., et al. (2015). Eight-year climatology of dust optical depth on Mars. *Icarus*, *251*, 65–95. <https://doi.org/10.1016/j.icarus.2014.12.034>

Montmessin, F., Korabiev, O., Lefèvre, F., Bertaux, J. L., Fedorova, A., Trokhimovskiy, A., et al. (2017). SPICAM on Mars Express: A 10 year in-depth survey of the Martian atmosphere. *Icarus*, *297*, 195–216. <https://doi.org/10.1016/j.icarus.2017.06.022>

Montmessin, F., & Lefèvre, F. (2013). Transport-driven formation of a polar ozone layer on Mars. *Nature*, *6*(11), 930.

O'Brien, K., Friedberg, W., Sauer, H. H., & Smart, D. F. (1996). Atmospheric cosmic rays and solar energetic particles at aircraft altitudes. *Environment International*, *22*(suppl. 1), S9–S44.

- Sheel, V., & Haider, S. A. (2016). Long-term variability of dust optical depths on Mars during MY24–MY32 and their impact on subtropical lower ionosphere: Climatology, modeling, and observations. *Journal of Geophysical Research: Planets*, *121*, 8038–8054. <https://doi.org/10.1002/2015JA022300>
- Smith, M. D. (2009). THEMIS observations of Mars aerosol optical depth from 2002–2008. *Icarus*, *202*(2), 444–452. <https://doi.org/10.1016/j.icarus.2009.03.027>
- Smith, M. D., Wolff, M. J., Clancy, R. T., Kleinböhl, A., & Murchie, S. L. (2013). Vertical distribution of dust and water ice aerosols from CRISM limb-geometry observations. *Journal of Geophysical Research: Planets*, *118*, 321–334. <https://doi.org/10.1002/jgre.20047>
- Steele, L. J., Lewis, S. R., Patel, M. R., Montmessin, F., Forget, F., & Smith, M. D. (2014). The seasonal cycle of water vapour on Mars from assimilation of Thermal Emission Spectrometer data. *Icarus*, *237*, 97–115. <https://doi.org/10.1016/j.icarus.2014.04.017>
- Thomas, P., & Gierasch, P. J. (1985). Dust devil on Mars. *Science*, *230*(4722), 175–177. <https://doi.org/10.1126/science.230.4722.175>
- Tolendo-Redondo, S., Salinas, A., Portí, J., Witasse, O., Cardnell, S., Fornieles, J., et al. (2017). Schumann resonances at Mars: Effects of the day-night asymmetry and dust loaded ionosphere. *Geophysical Research Letters*, *44*, 648–656. <https://doi.org/10.1002/2016GL071635>
- Trokhimovskiy, A., Fedrova, A., Korablev, O., Montmessin, F., Bertaux, J. L., Rodin, A., & Smith, M. D. (2015). Mars' water vapor mapping by SPICAM IR spectrometer: Five Martian years of observations. *Icarus*, *251*, 50–64. <https://doi.org/10.1016/j.icarus.2014.10.007>
- Whitten, R. C., Poppoff, I. G., & Sims, J. S. (1971). The ionosphere of Mars below 80 km altitude-I. Quiescent conditions. *Planetary and Space Science*, *19*(2), 243–250. [https://doi.org/10.1016/0032-0633\(71\)90203-0](https://doi.org/10.1016/0032-0633(71)90203-0)
- Willame, Y., Vandaele, A. C., Depiesse, C., Lefèvre, F., Letocart, V., Gillotay, D., & Montmessin, F. (2017). Retrieving cloud, dust and ozone abundances in the Martian atmosphere using SPICAM/UV nadir spectra. *Planetary and Space Science*, *142*, 9–25. <https://doi.org/10.1016/j.pss.2017.04.011>
- Wolff, M. J., Smith, M. D., Clancy, R. T., Arvidson, R., Kahre, M., Seelos, F., et al. (2009). Wavelength dependence of dust aerosol single scattering albedo as observed by the Compact Reconnaissance Imaging Spectrometer. *Journal of Geophysical Research*, *114*, E00D04. <https://doi.org/10.1029/2009JE003350>